

Seasonality in cholera dynamics: A rainfall-driven model explains the wide range of patterns in endemic areas

Theo Baracchini^a, Aaron A. King^b, Menno J. Bouma^{c,d}, Xavier Rodó^d,
Enrico Bertuzzo^e, Mercedes Pascual^{f,*}

^a*School of Architecture, Civil and Environmental Engineering, Ecole Polytechnique
Fédérale de Lausanne, Switzerland*

^b*Department of Ecology and Evolutionary Biology, University of Michigan, MI, United
States of America*

^c*Faculty of Public Health and Policy, London School of Hygiene and Tropical Medicine,
United Kingdom*

^d*Catalan Institute of Climate Sciences, Spain*

^e*Department of Environmental Sciences, Informatics and Statistics, University Ca'
Foscari, Venice, Italy*

^f*Department of Ecology and Evolution, University of Chicago, IL, United States of
America*

Abstract

Seasonal patterns in cholera dynamics exhibit pronounced variability across geographical regions, showing single or multiple peaks at different times of the year. Although multiple hypotheses related to local climate variables have been proposed, an understanding of this seasonal variation remains incomplete. The historical Bengal region, which encompasses the full range of cholera's seasonality observed worldwide, provides a unique opportunity to gain insights on underlying environmental drivers. Here, we propose a mechanistic, rainfall-temperature driven, stochastic epidemiological model which explicitly accounts for the fluctuations of the aquatic reservoir, and analyze

*Corresponding author

Email address: pascualmm@uchicago.edu (Mercedes Pascual)

Preprint submitted to Advances in Water Resources

November 23, 2016

with this model the historical dataset of cholera mortality in the Bengal region. Parameters are inferred with a recently developed sequential Monte Carlo method for likelihood maximization in partially observed Markov processes. Results indicate that the hydrological regime is a major driver of the seasonal dynamics of cholera. Rainfall tends to buffer the propagation of the disease in wet regions due to the longer residence times of water in the environment and an associated dilution effect, whereas it enhances cholera resurgence in dry regions. Moreover, the dynamics of the environmental water reservoir determine whether the seasonality is unimodal or bimodal, as well as its phase relative to the monsoon. Thus, the full range of seasonal patterns can be explained based solely on the local variation of rainfall and temperature. Given the close connection between cholera seasonality and environmental conditions, a deeper understanding of the underlying mechanisms would allow the better management and planning of public health policies with respect to climate variability and climate change.

Keywords: Infectious disease, modelling, cholera, seasonality, endemic, historical dataset, Bengal

1. Introduction

Although diarrheal diseases are preventable through suitable sanitary conditions, education and hygiene [46], they remain the second leading cause of mortality and are responsible for 20% of the deaths among children under 5 years of age [10]. In particular, although the treatment of cholera today is relatively easy and affordable, the disease remains a public health threat

7 across the globe, and an endemic problem in the estuary of the Ganges, its
8 native habitat.

9 A clear explanation for the diverse seasonal patterns of cholera outbreaks
10 in endemic areas has remained elusive [37]. Previous studies addressing the
11 role of climate drivers in disease dynamics have focused on interannual vari-
12 ability while prescribing the intra-annual seasonality [30]. The few proposed
13 explanations for seasonality have relied on complex environmental interac-
14 tions that vary with spatial location, involving regional hydrological models
15 [6], river discharge [28, 3], sea surface temperature [17, 7], and plankton
16 blooms [2, 15, 28]. No simple and unified mechanism based on *local* cli-
17 mate variables has been considered that can account for different seasonali-
18 ties within a region and across different regions of the world [20]. A better
19 understanding of seasonality in relation to climate variables would provide
20 a basis to better understand the effects of climate variability and climate
21 change in general.

22 Bangladesh and North-East India are endemic regions for cholera that
23 harbor the causing pathogen in the environment, the bacterium *V. cholerae*.
24 The interplay of high population density, seasonal hydroclimatology, flood-
25 plain geography and coastal ecology makes this region particularly vulnerable
26 to periodic outbreaks [3]. This region encompasses the most heterogeneous
27 temporal patterns of endemic cholera dynamics worldwide, ranging from a
28 single annual peak during or preceding the rainy season to a double peak in
29 the pre-and post-monsoon periods [34, 43] (Fig. 1). These patterns of recur-
30 rent outbreaks are still prevalent today in North-East India and Bangladesh,
31 as well as in various other regions of the world [23, 16, 20, 22]. If they have a

32 common explanation based on hydrology and local climate conditions, their
33 understanding can provide insights into the causes of endemicity and suggest
34 modifications of the environment to mitigate or eliminate disease burden
35 locally.

36 Through the analysis of a unique historical dataset containing 40 years of
37 monthly meteorological, demographic and epidemiological records, we pro-
38 pose a process-based model for the population dynamics of cholera driven
39 by local rainfall and temperature, and show that this model is able to cap-
40 ture the full range of seasonal patterns of this large estuarine region. The
41 transmission model explicitly accounts for volume fluctuations of the aquatic
42 reservoir and for the environmental bacterial concentration.

43 Although the crucial role played by the aquatic reservoir in the popula-
44 tion dynamics of the disease has already been widely assessed (e.g. [15, 37,
45 3, 34, 15, 38, 36, 7, 1, 27, 22, 4]), this work provides the first investigation of
46 the full range of seasonal incidence patterns with a simple process-based ap-
47 proach. The model combines the two opposing views on the dominant drivers
48 behind cholera epidemiological patterns [37]: that of the “localists” support-
49 ing a dominant role of the environment and of an environmental reservoir in
50 transmission, and that of the “contagionists”, emphasizing human-to-human
51 transmission and sanitary conditions. Mathematical models confronted to
52 time series data provide a useful tool to examine different hypotheses con-
53 cerning the climatic influences on disease dynamics, including the timing and
54 causes of seasonal patterns [5, 15]. They further provide a basis for climate-
55 based early warning systems, and for evaluating mitigation strategies for
56 environmentally driven infectious diseases [38].

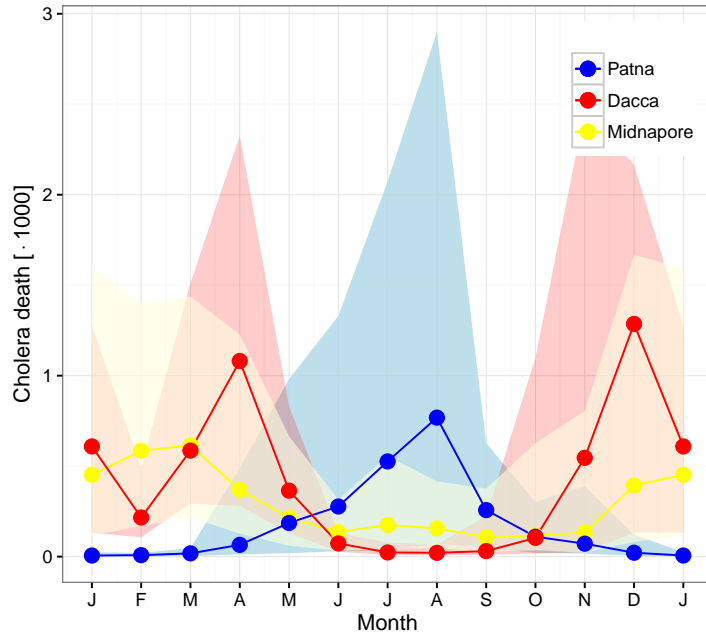


Figure 1: Three distinct cholera patterns representative of those found in the historical dataset as a whole: (1) a double peak, respectively pre- and post-monsoon, in the district of Dhaka; (2) a single wide peak from post- to pre-monsoon in the coastal district of Midnapore; and (3) a single annual peak during the monsoon in the drier north-western district of Patna. The lines correspond to the median of the monthly values, and the shaded areas, to the envelope of the data (bounded by the 10% and 90% quantiles) of the yearly values.

57 **2. Material and Methods**

58 *2.1. The historical dataset*

59 The former Bengal region constitutes the eastern part of the Indian sub-
 60 continent, and corresponds to the Indian state of West Bengal and the nation
 61 of Bangladesh today. It comprises the world’s largest delta and is the second
 62 most densely populated region around the globe. Besides Bengal, the study

63 area also includes the Indian states of Assam (north-east), Bihar (north-
64 west), Meghalaya and Tripura (east). Except for the dryer and mountainous
65 north-western parts, this tropical and humid region is a fertile alluvial plain.
66 The low elevation of the delta (Fig. 2) allows inland intrusions of salt water
67 during low river discharges.

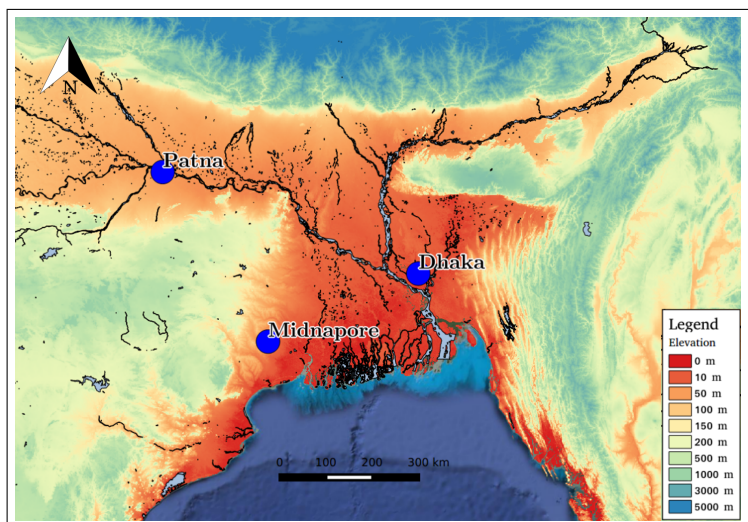


Figure 2: Elevation map of Bengal and its water bodies. Circles indicate the three representative districts presented in this paper.

68 An extensive data set on cholera deaths for 155 districts in 7 provinces
69 from 1891 through 1941 was collected from the records of the sanitary com-
70 missioners of the former British East Indian province of Bengal. A decadal
71 population census is also available for the same period. The published results
72 for 1891, 1901, 1911, 1921, 1931 and 1941 were linearly interpolated after cor-
73 rections for administrative changes. Monthly temperature and rainfall data
74 were also obtained from the India Weather Review, Annual Reports of the
75 Meteorological Department, Government of India, at the level of districts. A

76 monthly average was used for each location. Figure 3 illustrates the season-
 77 ality of these environmental variables for the three representative districts
 78 that are the focus of this study: Dhaka, Midnapore and Patna. (Although
 79 the methodology has been successfully tested for other districts, this work
 80 focuses on the three aforementioned ones whose representative seasonalities
 81 correspond to those of their respective regions, and cover the full range of
 82 observed seasonal patterns within the data set as a whole).

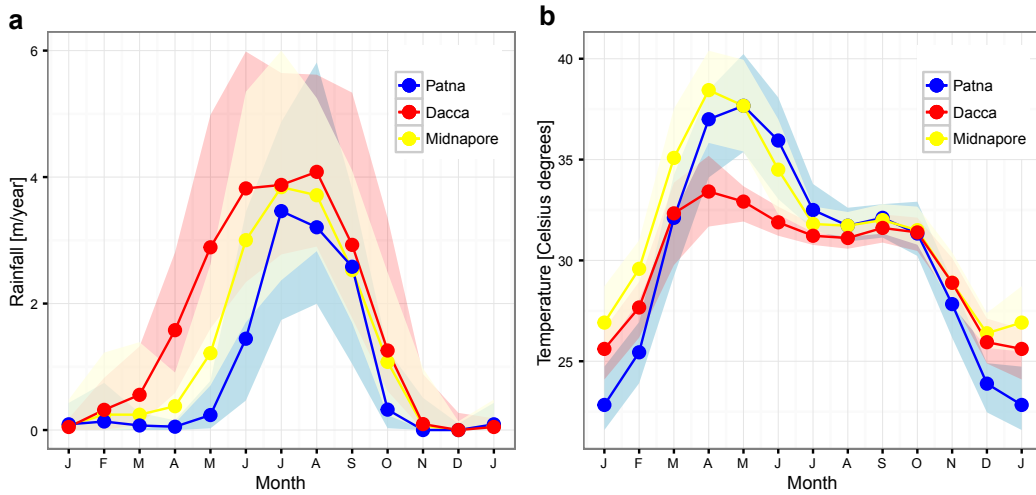


Figure 3: Seasonality of rainfall (a) and temperature (b) for three representative districts. The lines represent the median of the monthly variables across different years, whereas the shaded areas represent the envelope of the data (bounded by the 10% and 90% quantiles) of the yearly values.

83 2.2. Models

84 In this study we develop a non-linear, stochastic epidemiological model
 85 for cholera dynamics that builds upon previous efforts [30, 40, 6, 41]. The
 86 system is an expanded SIR-like model (for Susceptible-Infected-Recovered

87 classes of individuals) with 7 compartments (Fig. 4). The population of re-
 88 covered individuals is split into 3 compartments, to change the distribution
 89 of the duration of immunity from the typical exponential of models with a
 90 single recovery compartment, to a more realistic gamma distribution (with a
 91 characteristic duration or mode). This formulation provides a more flexible
 92 and realistic biological assumption, since an exponential distribution con-
 93 sideres an immune duration independent from the time since an individual
 94 has recovered [35]. Three compartments provide a proper trade-off between
 95 allowing the implementation of a gamma distribution while incurring a rea-
 96 sonable computational cost. The model has two additional state variables,
 97 not present in standard SIR formulations, for the population of pathogens in
 98 the aquatic environment and for the volume of the aquatic reservoir, respec-
 99 tively.

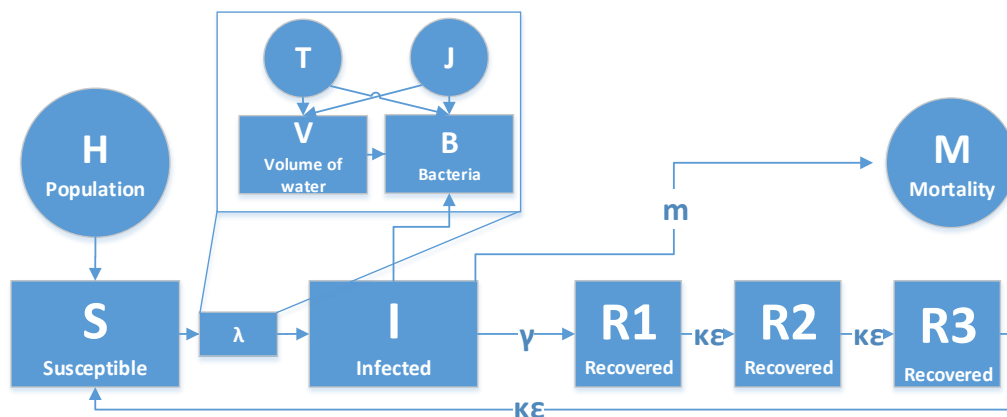


Figure 4: Diagram of the compartmental model. The rectangles correspond to the states variables and the circles, to observations that enter as environmental covariates (temperature and rainfall) or to the measurement variable (here, deaths). For simplicity, natural deaths are not included here in the diagram but are taken into account in the model.

100 Figure 4 depicts a diagram of this compartmental model. In this diagram,
 101 $S(t)$ denotes the number of susceptible individuals at time t , $I(t)$, the num-
 102 ber of infections, and $R_1(t)$, $R_2(t)$, $R_3(t)$ correspond to the multiple stages
 103 of recovery. $B(t)$ gives the bacterial abundance in the aquatic reservoir, and
 104 $V(t)$, the volume of this reservoir per unit area. In addition, $H(t)$ stands
 105 for the human population entering the system (births), $M(t)$, for the indi-
 106 viduals dying from cholera, $\lambda(t)$, for the force of infection, $T(t)$, for the local
 107 temperature, and $J(t)$, for the local rainfall. The diagram of Figure 4 can be
 108 written as the following set of coupled stochastic differential equations:

$$\frac{dS}{dt} = \kappa\epsilon R_3 + \mu H(t) + \frac{dH}{dt}(t) - (\lambda(t) + \mu)S \quad (1)$$

$$\frac{dI}{dt} = \lambda(t)S - (\gamma + m + \mu)I \quad (2)$$

$$\frac{dR_1}{dt} = \gamma I - (\kappa\epsilon + \mu)R_1 \quad (3)$$

$$\frac{dR_2}{dt} = \kappa\epsilon R_1 - (\kappa\epsilon + \mu)R_2 \quad (4)$$

$$\frac{dR_3}{dt} = \kappa\epsilon R_2 - (\kappa\epsilon + \mu)R_3 \quad (5)$$

$$\frac{dV}{dt} = J(t) - ET(T, V) - f(V) \cdot V \quad (6)$$

$$\frac{dB}{dt} = -\mu_B(T)B + p(t)[1 + \phi \cdot J(t)]I \cdot \xi(t) - f(V)B \quad (7)$$

109 where μ [s^{-1}] denotes the birth and mortality rate ($1/\mu$ is the life expectancy,
 110 fixed to 50 years), κ [-], the number of recovered compartments (here equal to
 111 3), ϵ [s^{-1}], the rate of immunity loss, $dH/dt(t)$, the observed changes in pop-
 112 ulation size, m [s^{-1}], the mortality rate due to disease, and γ [s^{-1}], the rate

113 of recovery from infection. The force of infection $\lambda(t)$ [s⁻¹] depends on the
 114 exposure rate β [s⁻¹] and on the environmental concentration of pathogens
 115 through a saturating function [15]:

$$\lambda(t) = \beta \frac{\frac{B(t)}{V(t)A}}{\frac{B(t)}{V(t)A} + K}, \quad (8)$$

116 where A [m²] is the geographical area in contact with the human population,
 117 and K is the half saturation concentration [#bacteria m⁻³].

118 The evolution of the volume of water per unit area V [m] is driven by the
 119 hydrological cycle (Eq. 6), namely by rainfall J [ms⁻¹], evapotranspiration
 120 ET [ms⁻¹] and drainage. Raw monthly rainfall data has been employed
 121 and interpolated to satisfy the daily time step of the model. The potential
 122 evapotranspiration (ET_p) is computed according to a re-calibrated Blaney-
 123 Criddle formula [9, 45, 44] based on historical temperature records. This
 124 modified form incorporates the new multiplicative and additive coefficients
 125 (0.35 and 2.5 respectively, in place of 0.46 and 8) re-calibrated to region-
 126 specific values by Sperna Weiland *et al.* [44]. This formula corresponds to the
 127 potential quantity of water that can be evapotranspired assuming that plants
 128 are in optimal conditions. When water availability is a limiting factor, the
 129 actual evapotranspiration ET decreases according to the following equation:

$$ET(T, V) = \begin{cases} ET_p(T) \cdot \frac{V(t)}{V_t} & \text{if } V(t) < V_t \\ ET_p(T) & \text{else,} \end{cases} \quad (9)$$

130 with V_t a calibrated parameter acting as a threshold for potential evap-
 131 otranspiration. This formulation used here allows regions with different
 132 environmental conditions to exhibit different evapotranspiration behaviors.
 133 Drainage corresponds to the flux of water leaving the area and it depends

134 on many factors, including soil type, topography, and the structure of the
 135 river network. Here it is modelled as a function of the volume V through a
 136 calibrated 3-parameter function describing the drainage rate $f(V)$:

$$f(V) = \delta \frac{V(t)^\alpha}{V(t)^\alpha + \tilde{V}^\alpha}. \quad (10)$$

137 The three parameters δ [s^{-1}], α [-] and \tilde{V} [m] flexibly change the behavior
 138 of the drainage function and allow different temporal scales of the responses
 139 to an increasing water volume (e.g. delayed or immediate drainage). These
 140 different responses allow the representation of the hydrological characteristics
 141 of different areas (e.g. mountainous versus estuarine).

142 The evolution of the environmental pool of bacteria (Eq. 7) results from
 143 a balance between contamination from infected individuals, pathogen death
 144 and drainage. The net death rate μ_B [s^{-1}] is assumed to be linearly dependent
 145 on temperature:

$$\mu_B(T) = \bar{\mu}_B \left(1 - \varepsilon \frac{T - \bar{T}}{T_{max} - \bar{T}} \right), \quad (11)$$

146 where the temperature is in degree Celsius. The parameter $\bar{\mu}_B$ [s^{-1}] de-
 147 notes the average death rate of the bacterium, ε [-], the dependency on tem-
 148 perature, and \bar{T} [$^{\circ}C$] and T_{max} [$^{\circ}C$] correspond respectively to the mean and
 149 maximum temperature of the studied area over the 40 years. When ε is larger
 150 than one, the death rate can become negative which describes the possible
 151 reproduction of bacteria in the environment at high temperature. The input
 152 from infected individuals is modeled through the term $p(t)[1 + \phi \cdot J(t)]I \cdot \xi(t)$
 153 where $p(t)$ is the *per capita* rate at which infected individuals shed bacteria

154 that contaminate the environmental reservoir. As the cholera time series
 155 indicate a long-term decrease in the number of deaths in some districts, we
 156 assume that sanitary conditions, represented by the parameter p [-], can
 157 potentially change and model this process through an exponential function
 158 $p(t) = p_0 e^{-d(t-\bar{t})}$, where \bar{t} [s] corresponds to the middle of the simulation
 159 period and p_0 [-] and d [s^{-1}] are two calibration parameters. The contam-
 160 ination process is assumed to be enhanced by rainfall which can wash out
 161 contaminated sites and deliver bacteria to the water reservoir [41, 18]. This
 162 input is accounted for by the parameter ϕ [sm^{-1}] [41]. Finally, $\xi(t)$ is the
 163 process noise of the model, with $\xi(t) = \frac{dW}{dt}$ and $dW \sim \Gamma_{WhiteNoise}(\mu_W, dt)$
 164 (μ_W equals the non-zero expected value, fixed here to 0.015 after an initial
 165 calibration of the model to the different districts). The last term, $f(V) \cdot B$,
 166 accounts for the bacteria within the water reservoir leaving the area through
 167 drainage.

168 By normalizing bacterial counts as $B^* = B/(KA)$, three parameters (p_0 ,
 169 K and A) are grouped into a single one, namely the ratio $\theta_0 = p_0/(KA)$,
 170 which reduces the number of parameters to be estimated. It follows that Eq.
 171 7 becomes $\frac{dB^*}{dt} = -\mu_B(T)B^* + \theta[1 + \phi \cdot J(t)]I \cdot \xi(t) - f(V)B^*$, and that the
 172 force of infection is given by $\lambda(t) = \beta \frac{B^*(t)/V(t)}{B^*(t)/V(t)+1}$.

173 The measurement model relates the deaths generated by the process
 174 model (the above-described differential equations for the 7 compartments
 175 SIR-like model), to those observed in the data, y_n , and allows one to compute
 176 a likelihood for the model given the observations. In a monthly time step, the
 177 number of new cholera deaths in the n^{th} interval is $M_n = m \int_{(n-1)/12}^{n/12} I(t)dt$
 178 (with t in years). The log-likelihood of each data point y_n is obtained through

179 a negative binomial distribution as:

$$\log(\mathcal{L}) = \log(\text{NegBinom}(y_n; \rho M_n, \frac{1}{\text{overdisp}^2})), \quad (12)$$

180 with mean ρM_n (where ρ [-] is the reporting rate) and variance $(\rho M_n / \text{overdisp})^2$,
181 with *overdisp* [-] a dispersion parameter. The negative binomial distribution
182 allows more overdispersion than that of the Poisson distribution.

183 2.3. Parameter inference

184 Parameter inference for nonlinear systems of stochastic differential equa-
185 tions has recently been facilitated by the development of methods for maxi-
186 mizing the likelihood via Iterated Filtering (MIF) [26, 25]. This frequentist
187 method is based on a particle filter approach developed by Ionides *et al.* [25],
188 which allows the estimation of parameters via simulation of the model (via
189 sequential Monte Carlo). Iterating filtering allows for models with measure-
190 ment error, non-stationarity, irregular sampling intervals, and the inclusion
191 of covariates. It also allows for hidden variables, that is variables for which
192 observations are unavailable, such as the number of susceptible individuals.
193 Moreover, the method has the advantage of focusing adaptively on favor-
194 able regions of the state-space, and can cope with a broad range of state
195 and noise distributions. Iterated filtering is implemented in the R statistical
196 open-source computing environment within the package *POMP* [29]. The
197 stochastic equations were integrated using the Euler-Maruyama algorithm.
198 For detailed description of the fitting algorithm see [25], and for a previous
199 application and explanation of the algorithm in the context of a climate-
200 driven model see [33]. In this study, 15 unknown parameters are estimated
201 using the 40 years time series of reported cholera deaths.

202 **3. Results**

203 *3.1. Parameters estimation*

204 Table 1 provides a summary of the fitted parameters for each district
 205 obtained after an initial broad search and an additional local refining of this
 206 search.

	Dhaka	Patna	Midnapore
V_t [m]	0.49	5.66	4.59
α [-]	19.85	4.91	14.96
\tilde{V} [m]	1.87	1.27	3.42
δ [y^{-1}]	5.04	474.35	553.43
$\bar{\mu}_B$ [y^{-1}]	317.49	107.59	368.20
ε [-]	0.16	0.02	0.02
θ_0 [y^{-1}]	0.0036	0.0036	0.0877
ϕ [y/m]	0.0148	0.1646	0.0298
$1/\epsilon$ [y]	5.43	6.73	4.88
$1/\gamma$ [d]	3.01	1.57	1.20
d [y^{-1}]	0.0000	0.0109	0.0072
<i>overdisp</i> [-]	0.82	0.79	0.52
ρ [-]	0.10	0.40	0.71
β [y^{-1}]	87.29	2.60	2.15
m [y^{-1}]	23.70	43.43	42.12

Table 1: Maximum likelihood parameters for each district.

207 *3.2. Seasonality*

208 Figure 5a shows the median monthly cholera deaths for 40 years of data
209 and the corresponding simulation from 1900 to 1940 (1890 to 1930 for Mid-
210 napore). The seasonality exhibits the typical bi-modal pattern of cholera
211 observed in the district of Dhaka. The two pre- and post-monsoon peaks
212 fall respectively in spring and autumn, with corresponding maxima in April
213 and December, as expected for the Classical biotype of the pathogen (the
214 current El Tor biotype emerged later in the region). The seasonality is well
215 captured by the model, with the peaks in phase with the data. The median
216 of the simulations also compares well with that of the data, except for a slight
217 underestimation of the fall peak. Although the envelope of the model does
218 include this variability, it overestimates the winter and spring infections. The
219 absence of reported deaths during summer is well captured by the model.

220 The single annual peak pattern observed during the monsoon in the north-
221 western and drier region of Patna, is also captured by the model (Fig. 5b).
222 The medians overlap well with the data, except for the month of August,
223 when the simulation underestimates the observed deaths. The envelope of
224 the data has a more negatively skewed distribution, with a sharp decrease
225 after August, whereas the one of the model is more symmetrical. Finally,
226 when no cases are observed between January and March, some sporadic
227 deaths are found in the simulations based on its envelope.

228 The coastal area of Midnapore shows another interesting pattern, a single
229 wider peak in the late winter-early spring. Once again, the dynamics are
230 captured by the model. Generally, a slight underestimation is observed in
231 the median and in the envelope in late autumn and early winter.

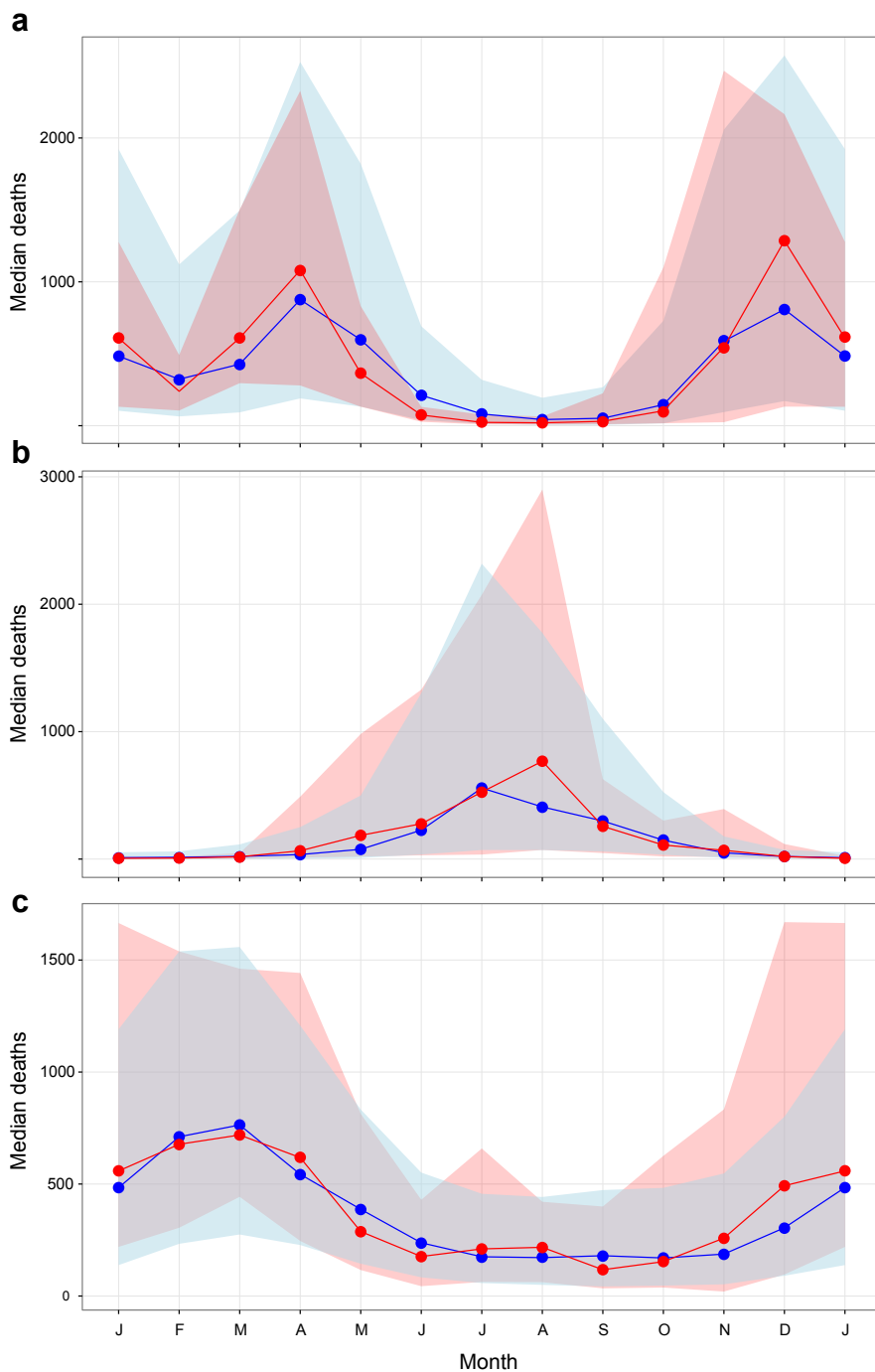


Figure 5: Cholera seasonality for the districts of Dhaka (a), Patna (b) and Midnapore (c). The median (solid lines) and envelope (shaded areas, monthly median of the 10% and 90% quantiles of the 250 simulated distributions) are shown for cholera mortality, to compare observations (in red) to model simulations (the result of 250 runs with the MLE parameter set) (blue).

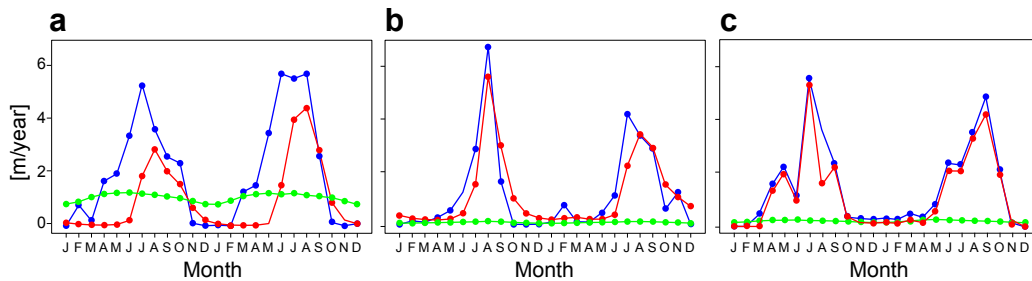


Figure 6: Hydrological fluxes for Dhaka (a), Patna (b) and Midnapore (c) for 2 representative years (respectively 1917-1918, 1914-1915 and 1902-1903). Rainfall (blue), drainage f(V) (red), and evapotranspiration (green).

232 Figure 6 shows the different fluxes controlling the water reservoir state
 233 (rainfall, evapotranspiration, and drainage) over a period of 2 years. The
 234 model suggests a much lower evapotranspiration in Patna than in the estu-
 235 arine region of Dhaka. Interestingly, the drainage has a faster response and
 236 a behaviour that closely tracks rainfall in the dry-northern district, whereas
 237 a delay is present in the wet-southern areas together with lower values. Mid-
 238 napore shows an intermediate pattern with low evapotranspiration, a fast
 239 drainage increase after a rainfall event, followed by a faster decay than that
 240 in Patna.

241 3.3. Interannual variability

242 Figure 7 compares the time series of the data to those from the simula-
 243 tions. (We note that these values do not represent next step prediction but
 244 the result of a set of 40-year simulations from estimated initial conditions).
 245 For the districts of Dhaka and Patna, the median of the model captures
 246 partially but not fully the interannual variation. Dhaka is more subject to
 247 frequent large outbreaks, and only a few of these are fully captured by the

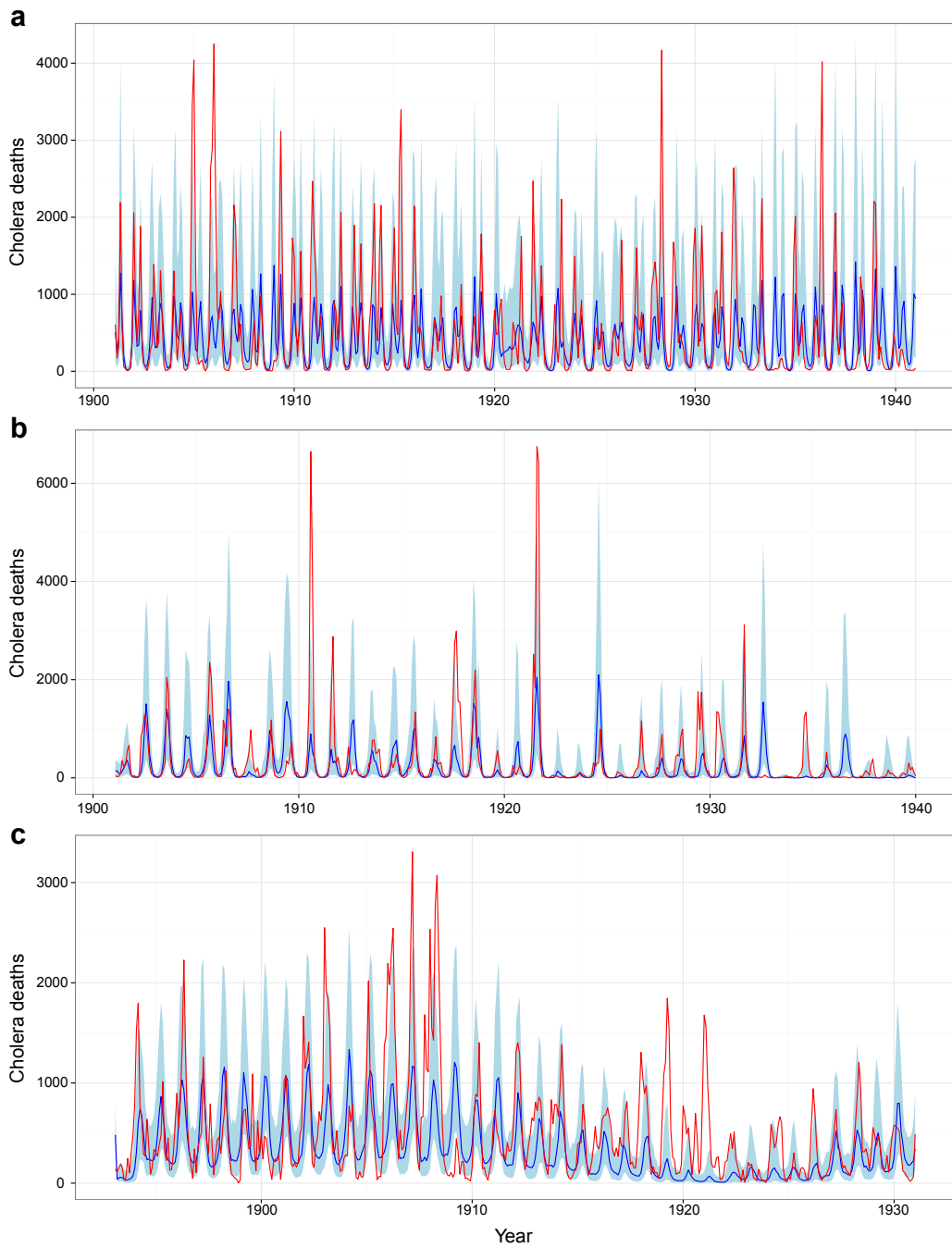


Figure 7: Time-series of the median of 250 simulations (blue) with the envelope (light blue, bounded by the 10% and 90% quantiles of the 250 simulated distributions), together with the cholera mortality data (red) for Dhaka (a), Patna (b) and Midnapore (c).

248 median of the simulations. Patna exhibits less frequent violent epidemics, al-
249 though two of them, in 1910 and 1921, are of particular intensity (exceeding
250 6500 monthly cholera deaths). Almost every important outbreak is within
251 the envelope of the model, suggesting that the model is capable of producing
252 those behaviors, but that stochasticity determines their exact timing and the
253 resulting variation results in the lower median. Finally, it is worth mentioning
254 that although average mortality appears more constant over time for Dhaka,
255 a slight downward trend is observed for Patna as reflected in parameter d of
256 Table 1. For Midnapore, the results are less clear, as important outbreaks
257 between 1900 and 1910 together with a temporary phase of milder infections
258 in 1922-1925 give an impression of a downward trend in time. This trend is
259 reflected in parameter d , which is slightly positive.

260 To assess quantitatively the interannual variation of the data, Singular
261 Spectrum Analysis (SSA), a statistical method decomposing the time series
262 into (orthogonal) principal components, was used to remove the seasonal
263 component of the time series, to extract the interannual variation ([8]; see
264 [39, 42] for examples of applications in epidemiology in the context of cli-
265 mate variability). Subsequent Fourier analysis of the interannual component
266 identified dominant periods of the anomalies in reported deaths of 4.2 and
267 7.8 years for Dhaka, 4.2 and 6 years for Patna, and 7.8 years for Midna-
268 pore. No evident link with the periodicity of the anomalies in the rainfall or
269 temperature could be detected.

270 4. Discussion

271 The proposed model explains the first seasonal outbreak in Dhaka by the
272 increase in temperature and associated drier conditions of spring, which in
273 turn increase pathogen concentration in the aquatic reservoir. This finding
274 offers an alternative hypothesis to that of Akanda *et al.* [2], who propose
275 that the first peak is mainly modulated by coastal hydroclimatic conditions
276 (salinity, plankton abundance) and the intrusion of salt water inland, during
277 periods of low river discharge (spring). Here, hydrological conditions alone
278 suffice to explain this characteristic pattern in Dhaka, and the full variation
279 of seasonalities across the extensive Bengal region.

280 Moreover, for Dhaka, the important summer rains would induce a dilu-
281 tion effect, presumably lowering incidence, as suggested by Emch *et al.* [21]
282 for cholera in Bangladesh. The peak stream flow observed in June creates
283 important inundations spreading the pathogen across the landscape. Given
284 the presence of water bodies in this estuarine region and the low drainage
285 suggested by the model, conditions of large scale contamination would be ex-
286 pected, with the bacterial population thriving locally without being washed
287 out from the area. This persistence would set the stage for a new outbreak
288 once the rainy season is over, the concentration of pathogen increases, and
289 the susceptible pool is replenished. This explanation is in accordance with
290 the more complex hypotheses in the literature (e.g. [28]) relying on impor-
291 tant discharges during the monsoon, lower salinity levels and pH, and high
292 nutrient loads of the water sources, which in turn favor plankton blooms and
293 bacterial growth. Finally the decline in cholera infection observed in January
294 and February is found to be temperature related, as suggested by Pascual *et*

295 *al.* [37]. However, the bacteria can survive through the winter in the aquatic
296 reservoir and be ready to initiate a new outbreak the following year [24, 14].

297 Rainfall in the model is found to buffer the propagation of the disease in
298 wet regions due to a dilution effect, while enhancing cholera resurgence in
299 dry regions. The more important drainage rate found in the dryer district
300 of Patna suggests higher discharges, possibly leading to the breakdown of
301 sanitary conditions and the boosting of transmission. This completely oppo-
302 site pattern to that of Dhaka is consistent with the observation that “overall
303 water levels matter and appear to determine whether the effect of rainfall
304 is positive or negative” [37]. It further emphasizes the importance of the
305 hydrological regime and of the water reservoir to cholera dynamics.

306 The model is also able to capture some of the interannual variability of
307 cholera based on rainfall and temperature. Although particularly explosive
308 outbreaks are above the median of the simulations, these anomalies do fall
309 within the envelopes of the model.

310 The results of Singular Spectrum Analysis suggest a role of stochasticity
311 in explaining the timing of these abnormally large outbreaks, at the same
312 time that they also indicate the existence of regularity in the form of some
313 detected periodicity above one year. Indeed the periodicity found in the
314 anomalies (of the interannual component) of reported deaths implies an in-
315 terplay with other climatic or demographic events. Interestingly, the period-
316 icity roughly corresponds to the dominant frequency of El Niño (about $1/4$
317 years^{-1}), the most important driver of interannual climate variability on a
318 global scale. This is in accordance with other findings [39, 42], where the
319 authors conclude that cholera dynamics are associated with a remote forcing

320 by ENSO (El Niño Southern Oscillation). For example, after the warming of
321 the Pacific, changes in cloud cover, evaporation, and increased heat flux can
322 be observed a few months later in the Bay of Bengal, thus linking general
323 climate to local variables impacting cholera [31]. Other studies also found
324 a link between ENSO and the regional climate of Bangladesh by studying
325 changes in the monsoon circulation over the area, their associated precipita-
326 tions changes and the possible implications for cholera incidence [11, 12, 13].
327 Consistent with our findings, an influence of ENSO on cholera would have
328 been weaker than in more recent decades, as it was previously described as
329 non-stationary in time, and was mainly observed for the more recent decades
330 and between 1900 and 1940 exclusively for the spring-peak (February to June)
331 [7]. Nevertheless, ENSO would have exerted an influence on the climate of
332 the Indian Ocean during the colonial period.

333 Patna shows a decline of both the reported and simulated cases over
334 time. Although several hypotheses can be formulated to explain this long
335 term trend, not much can be done to assess them. One explanation would
336 be a change of the reporting rate over time (with changes in administration,
337 demography, etc.). Cholera mortality rates in hospitals, for example, are
338 known to have decreased over this period [32]. Also, an improvement of
339 sanitation in Bengal, reducing cholera prevalence and deaths, is the most
340 likely explanation. Regardless, the long-term trend is well captured by the
341 model through the parameter d (Eq. 7).

342 Besides its application to the three chosen districts, the approach has
343 general applicability to other locations within the larger region. Other dis-
344 tricts were fitted successfully with the same model, including Chittagong and

345 Parganas. For the coastal district of Parganas, we obtained consistent results
346 to those of its close neighbour Midnapore, whose dynamics are also similar
347 (Parganas exhibits some differences, including a lower count of summer infec-
348 tions and a strong decreasing trend over time). For Northern districts, such
349 as Lakhimpur, their strongly epidemic dynamics with intermittent outbreaks
350 were only partially captured by the model. This kind of district would re-
351 quire an extension of the model that explicitly incorporates extinctions and
352 re-invasions.

353 Importantly the seasonal patterns considered here are still observed to-
354 day in the Bengal region, in Bangladesh and North-East India [23, 16, 20],
355 and in other regions of the world, as described in the global review of sea-
356 sonal cholera patterns for the period between 1974 and 2005 by Emch *et*
357 *al.* [20]. For example, cholera infections peak during the rainy season in
358 the Philippines, Costa Rica, Lesotho, and Gambia [23, 16]; they peak during
359 the summer in South America [34], and after the rainy season in Amazonia,
360 Brazil [15]. Furthermore the rather unique double peak of historical Dhaka
361 for the classical biotype, has been observed also for the more recent El Tor
362 biotype, and for the temporarily emergent strain, *Vibrio cholerae* O139, in
363 1993 in Bangladesh [19].

364 5. Conclusion

365 For two hundred years, an explanation for the range of seasonal patterns
366 in cholera based on local and simple environmental drivers has remained elu-
367 sive. Despite numerous studies of the association between climate variability
368 and incidence, no unified mechanisms explaining the temporal patterns in en-

369 demic regions have been proposed for cholera. Because the ecology of *Vibrio*
370 *cholerae* and the relative importance of its different transmission pathways
371 (human-to-human and environmental-to-human) are not fully understood,
372 there has been a sense that simple environmental drivers cannot explain the
373 diverse seasonal patterns of the disease. This study shows that a mechanistic
374 model including the explicit influence of rainfall and temperature is capable
375 to capture the full range of cholera seasonal patterns present in the historical
376 Bengal region.

377 Based on an SIR-like model with additional compartments for the water
378 volume and the pathogen concentration, insights were gained on the condi-
379 tions creating endemicity and variation in seasonal patterns. In particular,
380 the hydrological regime proved to be a dominant driver determining the sea-
381 sonal dynamics, with rainfall exerting different effects in different regions.
382 Specifically, rainfall can enhance transmission in dry regions, while buffering
383 the propagation of the disease in wet regions due to a dilution effect. Such
384 opposite influences indicate that overall water levels matter and act in com-
385 plex ways to determine whether the effect of rainfall is positive or negative.
386 Persistence of the disease is enabled by the environmental reservoir, which
387 underlies endemicity.

388 Although cholera today does no longer exert the global death toll it
389 once did, it remains responsible for substantial public health burdens in
390 Bangladesh and many developing countries. The dynamics behind its sea-
391 sonality have been shown to be closely associated with climate and environ-
392 mental variability. An understanding of environmental influences based on
393 hydrology could contribute to the better management and planning of public

394 health policies. Informing those capabilities in this way has become today
395 of paramount importance, given on-going changes in climate, including ex-
396 tremes, and their expected impact on the population dynamics of infectious
397 diseases. The changing environment, as the result not just of climate but
398 also urbanization and higher population densities, will lead to new societal
399 and scientific challenges in disease prevention and mitigation strategies.

400 **Acknowledgments**

401 EB acknowledges the support from the Swiss National Science Foundation
402 (SNF/FNS) project “Dynamics and controls of large-scale cholera outbreaks”
403 (DYCHO CR23I2 138104). MP and AAK are grateful for the support of
404 the National Oceanic and Atmospheric Administration’s Program on Oceans
405 and Health (Grant # F020704), and earlier support by the National Science
406 Foundation (NSF) through the program on the Ecology of Infectious Diseases
407 (Grant # 0430120). XR acknowledges the project New Indigo (“Intestinal
408 parasites in northern India”, PCIN-2013-038). The authors acknowledge
409 Leonard Evequoz for preliminary efforts on data and modelling. This research
410 was supported in part through computational resources and services provided
411 by Advanced Research Computing at the University of Michigan, Ann Arbor.

412 **Bibliography**

- 413 [1] Acosta, C. J., Galindo, C. M., Kimario, J., Senkoro, K., Urassa, H.,
414 Casals, C., Corachn, M., Eseko, N., Tanner, M., Mshinda, H., 2001.
415 Cholera outbreak in southern Tanzania: risk factors and patterns of
416 transmission. *Emerging infectious diseases* 7 (3), 583.

- 417 [2] Akanda, A. S., Jutla, A. S., Alam, M., de Magny, G. C., Siddique, A. K.,
418 Sack, R. B., Huq, A., Colwell, R. R., Islam, S., 2011. Hydroclimatic
419 influences on seasonal and spatial cholera transmission cycles: Implica-
420 tions for public health intervention in the Bengal Delta: Hydroclimatic
421 Influences on Seasonal Cholera. *Water Resources Research* 47 (3).
- 422 [3] Akanda, A. S., Jutla, A. S., Islam, S., 2009. Dual peak cholera transmis-
423 sion in Bengal Delta: A hydroclimatological explanation. *Geophysical*
424 *Research Letters* 36 (19).
- 425 [4] Ali, M., Emch, M., Donnay, J.-P., Yunus, M., Sack, R. B., 2002. Ident-
426 ifying environmental risk factors for endemic cholera: a raster GIS ap-
427 proach. *Health & place* 8 (3), 201–210.
- 428 [5] Altizer, S., Dobson, A., Hosseini, P., Hudson, P., Pascual, M., Rohani,
429 P., 2006. Seasonality and the dynamics of infectious diseases: Seasonality
430 and infectious diseases. *Ecology Letters* 9 (4), 467–484.
- 431 [6] Bertuzzo, E., Mari, L., Righetto, L., Gatto, M., Casagrandi, R.,
432 Rodriguez-Iturbe, I., Rinaldo, A., 2012. Hydroclimatology of dual-peak
433 annual cholera incidence: Insights from a spatially explicit model. *Geo-*
434 *physical Research Letters*.
- 435 [7] Bouma, M. J., Pascual, M., 2001. Seasonal and interannual cycles of
436 endemic cholera in Bengal 1891-1940 in relation to climate and geogra-
437 phy. In: *The Ecology and Etiology of Newly Emerging Marine Diseases*.
438 Springer, pp. 147–156.

- 439 [8] Broomhead, D. S., King, G. P., Jun. 1986. Extracting qualitative dynam-
440 ics from experimental data. *Physica D: Nonlinear Phenomena* 20 (2),
441 217–236.
- 442 [9] Brouwer, C., Heibloem, M., 1986. Irrigation Water Management: Irri-
443 gation Water Needs. Food and Agriculture Organization - Natural Re-
444 sources Management and Environment Department.
- 445 [10] Bryce, J., Boschi-Pinto, C., Shibuya, K., Black, R. E., 2005. WHO
446 estimates of the causes of death in children. *The Lancet* 365 (9465),
447 1147–1152.
- 448 [11] Cash, B. A., Rod, X., Kinter, J. L., Sep. 2008. Links between Tropical
449 Pacific SST and Cholera Incidence in Bangladesh: Role of the Eastern
450 and Central Tropical Pacific. *Journal of Climate* 21 (18), 4647–4663.
- 451 [12] Cash, B. A., Rod, X., Kinter, J. L., Apr. 2009. Links between Tropical
452 Pacific SST and Cholera Incidence in Bangladesh: Role of the Western
453 Tropical and Central Extratropical Pacific. *Journal of Climate* 22 (7),
454 1641–1660.
- 455 [13] Cash, B. A., Rod, X., Kinter, J. L., Yunus, M., May 2010. Disentangling
456 the Impact of ENSO and Indian Ocean Variability on the Regional Cli-
457 mate of Bangladesh: Implications for Cholera Risk. *Journal of Climate*
458 23 (10), 2817–2831.
- 459 [14] Chun, J., Grim, C. J., Hasan, N. A., Lee, J. H., Choi, S. Y., Haley,
460 B. J., Taviani, E., Jeon, Y.-S., Kim, D. W., Lee, J.-H., Brettin, T. S.,
461 Bruce, D. C., Challacombe, J. F., Detter, J. C., Han, C. S., Munk,

- 462 A. C., Chertkov, O., Meincke, L., Saunders, E., Walters, R. A., Huq, A.,
463 Nair, G. B., Colwell, R. R., 2009. Comparative genomics reveals mecha-
464 nism for short-term and long-term clonal transitions in pandemic *Vibrio*
465 *cholerae*. *Proceedings of the National Academy of Sciences* 106 (36),
466 15442–15447.
- 467 [15] Codeço, C. T., 2001. Endemic and epidemic dynamics of cholera: the
468 role of the aquatic reservoir. *BMC infectious diseases* 1 (1), 1.
- 469 [16] Collins, A. E., 1996. The geography of cholera. In: Drasar, P. B. S.,
470 Forrest, D. B. D. (Eds.), *Cholera and the Ecology of *Vibrio cholerae**.
471 Springer Netherlands, pp. 255–294, doi: 10.1007/978-94-009-1515-2_8.
- 472 [17] Colwell, R. R., 1996. Global climate and infectious disease: The cholera
473 paradigm. *Science* 274 (5295), 2025–2031.
- 474 [18] Eisenberg, M., Kujbida, G., Tuite, A., Fisman, D., Tien, J., 2013. Exam-
475 ining rainfall and cholera dynamics in haiti using statistical and dynamic
476 modeling approaches. *Epidemics* 5 (4), 197–207.
- 477 [19] Emch, M., Ali, M., Feb. 2001. Spatial and Temporal Patterns of Di-
478 arrheal Disease in Matlab, Bangladesh. *Environment and Planning A*
479 33 (2), 339–350.
- 480 [20] Emch, M., Feldacker, C., Islam, M. S., Ali, M., 2008. Seasonality of
481 cholera from 1974 to 2005: a review of global patterns. *International*
482 *Journal of Health Geographics* 7 (1), 31.
- 483 [21] Emch, M., Feldacker, C., Yunus, M., Streatfield, P. K., Thiem, V. D.,
484 Canh, D. G., Ali, M., 2008. Local environmental predictors of cholera in

- 485 Bangladesh and Vietnam. *American Journal of Tropical Medicine and*
486 *Hygiene* 78 (5), 823–832.
- 487 [22] Emch, M., Yunus, M., Escamilla, V., Feldacker, C., Ali, M., 2010. Local
488 population and regional environmental drivers of cholera in Bangladesh.
489 *Environmental Health* 9 (1), 2.
- 490 [23] Gangarosa, E. J., Mosley, W. H., 1974. Epidemiology and surveillance
491 of cholera. *Cholera*. Philadelphia: WB Saunders, 381–403.
- 492 [24] Huq, A., Sack, R. B., Nizam, A., Longini, I. M., Nair, G. B., Ali, A.,
493 Morris, J. G., Khan, M. N. H., Siddique, A. K., Yunus, M., Albert,
494 M. J., Sack, D. A., Colwell, R. R., 2005. Critical Factors Influencing
495 the Occurrence of *Vibrio cholerae* in the Environment of Bangladesh.
496 *Applied and Environmental Microbiology* 71 (8), 4645–4654.
- 497 [25] Ionides, E. L., Bhadra, A., Atchad, Y., King, A., 2011. Iterated filtering.
498 *The Annals of Statistics* 39 (3), 1776–1802.
- 499 [26] Ionides, E. L., Bret, C., King, A. A., 2006. Inference for nonlinear
500 dynamical systems. *Proceedings of the National Academy of Sciences*
501 103 (49), 18438–18443.
- 502 [27] Jutla, A., Whitcombe, E., Hasan, N., Haley, B., Akanda, A., Huq, A.,
503 Alam, M., Sack, R. B., Colwell, R., 2013. Environmental Factors Influ-
504 encing Epidemic Cholera. *American Journal of Tropical Medicine and*
505 *Hygiene* 89 (3), 597–607.
- 506 [28] Jutla, A. S., Akanda, A. S., Griffiths, J. K., Colwell, R., Islam, S., Jan.

- 507 2011. Warming Oceans, Phytoplankton, and River Discharge: Implica-
508 tions for Cholera Outbreaks. *The American Journal of Tropical Medicine*
509 *and Hygiene* 85 (2), 303–308.
- 510 [29] King, A. A., Ionides, E. L., Breto, C., Kendall, E., Lavine, M., Reuman,
511 D. C., Wearing, H., Wood, S. N., 2013. Package ‘pomp’.
- 512 [30] King, A. A., Ionides, E. L., Pascual, M., Bouma, M. J., 2008. Inapparent
513 infections and cholera dynamics. *Nature* 454 (7206), 877–880.
- 514 [31] Klein, S. A., Soden, B. J., Lau, N.-C., 1999. Remote Sea Surface Tem-
515 perature Variations during ENSO: Evidence for a Tropical Atmospheric
516 Bridge. *Journal of Climate* 12 (4), 917–932.
- 517 [32] Koelle, K., Pascual, M., Jun. 2004. Disentangling Extrinsic from Intrin-
518 sic Factors in Disease Dynamics: A Nonlinear Time Series Approach
519 with an Application to Cholera. *The American Naturalist* 163 (6), 901–
520 913.
- 521 [33] Laneri, K., Bhadra, A., Ionides, E. L., Bouma, M., Dhiman, R. C., Ya-
522 dav, R. S., Pascual, M., Sep. 2010. Forcing Versus Feedback: Epidemic
523 Malaria and Monsoon Rains in Northwest India. *PLOS Comput Biol*
524 6 (9), e1000898.
- 525 [34] Lipp, E. K., Huq, A., Colwell, R. R., 2002. Effects of Global Climate on
526 Infectious Disease: the Cholera Model. *Clinical Microbiology Reviews*
527 15 (4), 757–770.
- 528 [35] Lloyd, A. L., May 2001. Destabilization of epidemic models with the

- 529 inclusion of realistic distributions of infectious periods. Proceedings of
530 the Royal Society B: Biological Sciences 268 (1470), 985–993.
- 531 [36] Miller, C., Feachem, R., Drasar, B., 1985. Cholera epidemiology in de-
532 veloped and developing countries: New thoughts on transmission, sea-
533 sonality, and control. *The Lancet* 325 (8423), 261–263.
- 534 [37] Pascual, M., Bouma, M. J., Dobson, A. P., 2002. Cholera and climate:
535 revisiting the quantitative evidence. *Microbes and infections* 4 (2), 237–
536 245.
- 537 [38] Pascual, M., Chaves, L., Cash, B., Rodó, X., Yunus, M., 2008. Predict-
538 ing endemic cholera: the role of climate variability and disease dynamics.
539 *Climate Research* 36, 131–140.
- 540 [39] Pascual, M., Rodó, X., Ellner, S. P., Colwell, R., J., B. M., 2000. Cholera
541 Dynamics and El Nino-Southern Oscillation. *Science* 289 (5485), 1766–
542 1769.
- 543 [40] Righetto, L., Casagrandi, R., Bertuzzo, E., Mari, L., Gatto, M.,
544 Rodriguez-Iturbe, I., Rinaldo, A., 2012. The role of aquatic reservoir
545 fluctuations in long-term cholera patterns. *Epidemics* 4 (1), 33–42.
- 546 [41] Rinaldo, A., Bertuzzo, E., Mari, L., Righetto, L., Blokesch, M., Gatto,
547 M., Casagrandi, R., Murray, M., Vesenbeckh, S. M., Rodriguez-Iturbe,
548 I., 2012. Reassessment of the 20102011 Haiti cholera outbreak and
549 rainfall-driven multiseason projections. *Proceedings of the National*
550 *Academy of Sciences* 109 (17), 6602–6607.

- 551 [42] Rodó, X., Pascual, M., Fuchs, G., Faruque, A. S. G., 2002. ENSO and
552 cholera: A nonstationary link related to climate change? Proceedings
553 of the national Academy of Sciences 99 (20), 12901–12906.
- 554 [43] Ruiz-Moreno, D., Pascual, M., Bouma, M., Dobson, A., Cash, B., 2007.
555 Cholera Seasonality in Madras (19011940): Dual Role for Rainfall in
556 Endemic and Epidemic Regions. *EcoHealth* 4 (1), 52–62.
- 557 [44] Sperna Weiland, F. C., Tisseuil, C., Durr, H. H., Vrac, M., van Beek, L.
558 P. H., 2012. Selecting the optimal method to calculate daily global ref-
559 erence potential evaporation from CFSR reanalysis data for application
560 in a hydrological model study. *Hydrology and Earth System Sciences*
561 16 (3), 983–1000.
- 562 [45] Weiss, M., Menzel, L., 2008. A global comparison of four potential evap-
563 otranspiration equations and their relevance to stream flow modelling in
564 semi-arid environments. *Advances in Geosciences* 18.
- 565 [46] WHO, 2015. Cholera, World Health Organisation. Accessed on: 2014-
566 04-08.
567 URL <http://www.who.int/mediacentre/factsheets/fs107/en>